

**Figure 4** The dependence of the spectral exponents of the phytoplankton (green) and zooplankton (red) populations on the model parameters. The low-resolution model, including only the largest eddies, was run repeatedly with values of  $\delta$  and  $\tau$  indicated, but using the same velocity field. The contoured spectral exponents were obtained by averaging the spectra derived from snapshots of the populations at 10-day intervals between 160 and 300 model days. Within the shaded region,  $\beta_z > \beta_p$ ; elsewhere, the zooplankton have a flatter spectra than the phytoplankton. The star marks the values of the parameters used in Figs 2 and 3.

larger zooplankton mortality leads to phytoplankton distributions with steeper spectra, because of the reduced grazing on the phytoplankton. Because the simplified physics, including only the largest eddies, is less efficient at transferring variability towards smaller length scales, the spectral slopes are steeper than the slopes generated by the model with a full turbulent cascade.

Detailed simulations, incorporating fluid-dynamic models of quasi-geostrophic turbulence, multi-compartment ecosystem dynamics, and seasonal forcing, have been attempted<sup>24</sup>. These simulations find a similar result: that the zooplankton have a flatter spectra than the phytoplankton. Because of the complexity of the processes represented, the source of the fine-scale zooplankton structure in those models is unclear. The power of a simple model is to demonstrate how populations with these different distributions may occur without the need for any mechanism beyond their different response rates to changes in the environment caused by turbulent advection. Although predicting spectral form is a weak test of any theory<sup>25</sup>, and the available evidence is perhaps ambiguous (not all data sets show flatly sloped zooplankton spectra<sup>26</sup>, and similar results may arise as observational artefacts<sup>27</sup>), this analysis suggests that zooplankton lifetime is an important determinant of their spatial pattern. A new observational sophistication, which enables zooplankton distributions to be tightly related to the physical properties of the surface waters<sup>28</sup>, will allow a detailed testing of these relationships. □

Received 3 June; accepted 22 September 1997.

1. Okubo, A. *Biomathematics* Vol. 10, *Diffusion and Ecological Problems: Mathematical Models* (Springer, Berlin, 1980).
2. Mackas, D. L. & Boyd, C. M. Spectral analysis of zooplankton spatial heterogeneity. *Science* **204**, 62–64 (1979).
3. Tsuda, A., Sugisaki, H., Ishimaru, T., Saino, T. & Sato, T. White-noise-like distribution of the oceanic copepod *Neocalanus cristatus* in the subarctic North Pacific. *Mar. Ecol. Prog. Ser.* **97**, 39–46 (1993).
4. Okubo, A. Oceanic diffusion diagrams. *Deep Sea Res.* **18**, 789–802 (1971).
5. Levin, S. A. & Segel, L. A. Hypothesis for origin of plankton patchiness. *Nature* **259**, 659 (1976).
6. Wroblewski, J. S. & O'Brien, J. J. A spatial model of phytoplankton patchiness. *Mar. Biol.* **35**, 161–175 (1976).
7. Steele, J. H. & Henderson, E. W. A simple model for plankton patchiness. *J. Plankton Res.* **14**, 1397–1403 (1992).
8. Malchow, H. Nonequilibrium structures in plankton dynamics. *Ecol. Model.* **75/76**, 123–134 (1994).
9. Parsons, T. R., Takahashi, M. & Hargrave, B. *Biological Oceanographic Processes*, 3rd edn (Pergamon, Oxford, 1984).
10. Kierstead, H. & Slobodkin, L. B. The size of water masses containing plankton blooms. *J. Mar. Res.* **12**, 141–147 (1953).
11. Klein, P. & Hua, B. L. The mesoscale variability of the sea surface temperature: An analytical and numerical model. *J. Mar. Res.* **48**, 729–763 (1990).

12. Kiorboe, T. & Sabatini, M. 1995 Scaling of fecundity, growth and development in marine planktonic copepods. *Mar. Ecol. Prog. Ser.* **120**, 285–298 (1995).
13. Denman, K. L. & Platt, T. The variance spectrum of phytoplankton in a turbulent ocean. *J. Mar. Res.* **34**, 593–601 (1976).
14. Gower, J. F. R., Denman, K. L. & Holyer, R. J. Phytoplankton patchiness indicates the fluctuation spectrum of mesoscale oceanic structure. *Nature* **288**, 157–159 (1980).
15. Lesieur, M. & Sadourny, R. Satellite-sensed turbulent ocean structure. *Nature* **294**, 673 (1981).
16. Bennett, A. F. & Denman, K. L. Phytoplankton patchiness: inferences from particle statistics. *J. Mar. Res.* **43**, 307–335 (1985).
17. Holloway, G. Eddies, waves, circulation and mixing: statistical geofluid mechanics. *Annu. Rev. Fluid Mech.* **18**, 91–147 (1986).
18. Powell, T. M. & Okubo, A. Turbulence, diffusion and patchiness in the sea. *Phil. Trans. R. Soc. Lond. B* **343**, 11–18 (1994).
19. Dyke, P. P. G. & Robertson, T. The simulation of offshore turbulent dispersion using seeded eddies. *Appl. Math. Model.* **9**, 429–433 (1985).
20. Trathan, P. N., Priddle, J., Watkins, J. L., Miller, D. G. M. & Murray, A. W. A. Spatial variability of Antarctic krill in relation to mesoscale hydrography. *Mar. Ecol. Prog. Ser.* **98**, 61–71 (1993).
21. Renka, R. J. Triangulation and interpolation at arbitrarily distributed points in the plane. *ACM Trans. Math. Software* **10**, 440–442 (1984).
22. Deschamps, P. Y., Frouin, R. & Wald, L. Satellite determinations of the mesoscale variability of the sea surface temperature. *J. Phys. Oceanogr.* **11**, 864–870 (1981).
23. Mackas, D. L., Denman, K. L. & Abbot, M. R. Plankton patchiness: biology in the physical vernacular. *Bull. Mar. Sci.* **37**, 652–674 (1985).
24. Smith, C. L., Richards, K. J. & Fasham, M. J. R. The impact of mesoscale eddies on plankton dynamics in the upper ocean. *Deep Sea Res.* **1** **43**, 1807–1832 (1996).
25. Armi, L. & Flament, P. Cautionary remarks on the spectral interpretation of turbulent flows. *J. Geophys. Res.* **C90**, 11779–11782 (1985).
26. Piontkovski, S. A. *et al.* Spatial heterogeneity of the planktonic fields in the upper mixed layer of the open ocean. *Mar. Ecol. Prog. Ser.* **148**, 145–154 (1997).
27. Fasham, M. J. R. in *Spatial Pattern in Plankton Communities* (ed. Steele, J. H.) 131–156 (Plenum, New York, 1978).
28. Gallagher, S. M., Davis, C. S., Epstein, A. W., Solow, A. & Beardsley, R. C. High-resolution observations of plankton spatial distributions correlated with hydrography in the Great South Channel, Georges Bank. *Deep Sea Res.* **II** **43**, 1627–1663 (1996).
29. Charney, J. G. Geostrophic turbulence. *J. Atmos. Sci.* **28**, 1087–1095 (1971).
30. Middleton, J. F. Drifter spectra and diffusivities. *J. Mar. Res.* **43**, 37–55 (1985).

**Acknowledgements.** I thank P. Boyd, P. Sutton, C. Stevens and J. Sharples for critical reading of the draft manuscript, and R. Renka for software made available through the TOMS internet archive that was used to interpolate the Lagrangian variables onto a regular grid.

Correspondence and requests for materials should be addressed to E.A. (e-mail: e.abraham@niwa.cri.nz).

## Collinear stimuli regulate visual responses depending on cell's contrast threshold

Uri Polat\*, Keiko Mizobe\*, Mark W. Pettet, Takuji Kasamatsu & Anthony M. Norcia

The Smith-Kettlewell Eye Research Institute, 2232 Webster Street, San Francisco, California 94115, USA

Neurons in the primary visual cortex are selective for the size, orientation and direction of motion of patterns falling within a restricted region of visual space known as the receptive field<sup>1</sup>. The response to stimuli presented within the receptive field can be facilitated or suppressed by other stimuli falling outside the receptive field which, when presented in isolation, fail to activate the cell<sup>2–8</sup>. Whether this interaction is facilitative<sup>3,4,7,9–12</sup> or suppressive<sup>2,3,5,6,8–14</sup> depends on the relative orientation of pattern elements inside and outside the receptive field. Here we show that neuronal facilitation preferentially occurs when a near-threshold stimulus inside the receptive field is flanked by higher-contrast, collinear elements located in surrounding regions of visual space. Collinear flanks and orthogonally oriented flanks, however, both act to reduce the response to high-contrast stimuli presented within the receptive field. The observed pattern of facilitation and suppression may be the cellular basis for the observation in humans that the detectability of an oriented pattern is enhanced by collinear flanking elements<sup>15–17</sup>. Modulation of neuronal responses by stimuli falling outside their receptive fields may thus represent an early neural mechanism for encoding objects and enhancing their perceptual saliency.

\* Present addresses: Institute for Vision Research, Ehad Ha'am 14, Rehovot 76105, Israel (U.P.); Department of Ophthalmology, Kyoto Prefectural University of Medicine, Hirokoji Kawara-machi, Kamigyo-ku, Kyoto 602, Japan (K.M.).

We recorded single-cell discharges extracellularly over a wide range of luminance contrasts to compare individual cells' contrast-response functions under four stimulus conditions: (1) a Gabor patch (discrete grating target) presented alone inside the classical receptive field (CRF) (Fig. 1a); (2) the CRF target plus two matching Gabor flanks that were well outside the CRF (Fig. 1b); and (3) the flanks alone (Fig. 1c). Orthogonally oriented flanks were also tested (Fig. 1d). The target-flank separation, centre-to-centre, was usually set at a 3–4 wavelength distance (the reciprocal of spatial frequency), because maximal perceptual facilitation occurs at this range<sup>15,16</sup>. Typical cellular behaviour is depicted in Fig. 2a, in which response magnitude was plotted as a function of logarithmic target contrast. When the CRF was stimulated by the target alone, response magnitude increased as target contrast increased, with some saturation at the highest contrast tested (Fig. 2a, filled circles).

A major finding was revealed when the cell was stimulated with compound stimuli made of the target on the CRF and two high-contrast (80%) collinear flanks placed well outside the CRF. The

response was facilitated at low target contrasts and suppressed at high target contrasts (Fig. 2a, open circles). No modulatory effects were seen at intermediate target contrasts. When stimulated with the two flanks alone, the cell's activity remained at the background noise level (Fig. 2a, flanks alone), because stimulation of the CRF surround did not drive the cell. A similar pattern of modulation of the contrast-response function was obtained in another cell when the contrast-response function was measured using the swept-contrast method (see Methods). When tested with the target plus collinear flanks, we again found facilitation of the response at low target contrasts and suppression at relatively high contrasts (Fig. 2b). The flanks presented in isolation failed to elicit a response (Fig. 2b, flanks alone).

In a population of 96 cells (39 simple and 44 complex cells, and 13 undecided cells) recorded from five adult cats, 83 cells were tested with three contrast values or more. Most of the 83 cells showed modulation of either both facilitation and suppression (~34%), facilitation alone (~33%) or suppression alone (19%), when tested with various combinations of stimulus parameters. A fraction of

**Table 1 Incidence of modulation types depending on stimulus types**

	Total	Orthogonal			Per cent
		Facilitation	No effect	Suppression	
Total	150	8	104	38	
Facilitation	29	5	21	3	19.3
Collinear	99	3	78	18	66.0
No effect	22	0	5	17	14.7
Suppression					
Per cent		5.3	69.3	25.3	100.0

Entries in each row and column indicate the number of responses ( $n = 150$ , from 34 cells) that showed the indicated modulation effect for the collinear and orthogonal flank stimuli, respectively. The asymptotic probability of the sample being drawn from a parent population that has identical response distributions for collinear and orthogonal flank stimuli was  $P < 0.00003$  (Bowker's test for off-diagonal symmetry;  $\chi^2 = 23.85$ , d.f. = 3). This low  $P$  value indicates significant asymmetry in the distribution of facilitation and suppression between the collinear and orthogonal flanks.

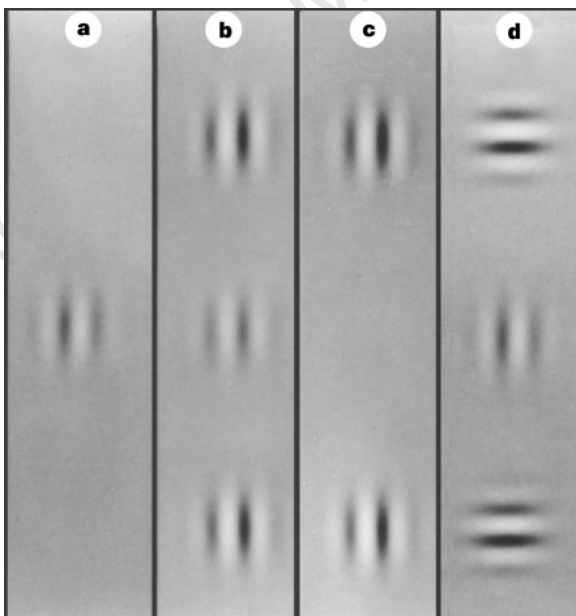


**Figure 1** The stimuli were Gabor patches (Gaussian-weighted sinusoids) presented singly or in combination. **a**, Target patch optimally fitted to the classical receptive field (CRF) in its size, location, orientation and spatial frequency. **b**, Target patch presented concurrently with two flanking patches having the same properties as the target except for their contrast (collinearity test). The flanks were located well outside the CRF. **c**, Two flanking patches presented alone. **d**, Target and two flanks with orthogonal orientation. All other test parameters were the same as in **b**.

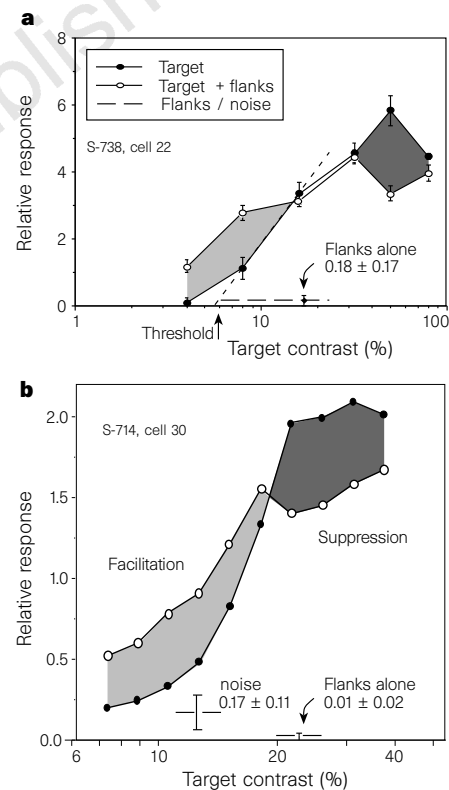


**Figure 2** The comparison of contrast-response functions between target alone (filled circles) and target plus two collinear flanks (open circles) is exemplified in two single cells. The x-axis represents the target contrast as a percentage and the y-axis the cell's response magnitude in relative units of Fourier transforms, which varied depending on cells, and which were not normalized across cells. **a**, In the collinear configuration, the cell's response was facilitated at low target contrasts and suppressed at high target contrasts. The contrast threshold of this cell was ~6%, as estimated by linear extrapolation of the linear portion of the contrast-response curve to the noise level. The flanks alone elicited an insignificant response. Each vertical bar refers to one standard error of the respective mean (s.e.m.). This complex cell, recorded 986  $\mu\text{m}$  from the cortical surface, had a moderate CRF size ( $3.2 \times 2.4$  deg). The average spike counts per run (9.7 s) at 8% contrast were as follows:  $314.3 \pm 59.2$  (target alone),  $488.5 \pm 42.5$  (target + flanks) and  $269.4 \pm 13.8$  (flanks alone). **b**, Contrast response functions of another cell. The contrast-response function was measured by the swept-contrast method (see Methods). The cell response was facilitated at low contrasts and suppressed at intermediate and high contrasts. This simple cell, recorded at 1,126  $\mu\text{m}$  from the cortical surface, had a relatively small CRF ( $1.0 \times 0.8$  deg).

cells showed no modulatory effects of the collinearly presented flanks (~14%).

In the 83 cells, we obtained 325 data points that satisfied a statistical test for significant modulation (target-flank additivity test, see Methods), covering three or more contrast values per cell. A population summary of the contrast-dependent modulation is shown for the collinear configuration in Fig. 3a. The distribution of the three modes of modulation (suppression, facilitation and no effect) was comparable between simple and complex cell populations (data not shown). Therefore, the two populations were combined using the first harmonic response for simple cells and the second for complex cells. For unclassified cells, the dominant harmonic was used. On average, two-fifths of the 325 data points accumulated from the 83 cells showed significant modulation, either suppression or facilitation, when tested with several target contrasts, the lowest being ~4% or lower, and the highest at 80%. The rest showed no modulation.

When the data were analysed separately within the modulated group, a suggestive trend emerged: facilitation was common at low contrasts and suppression was common at high contrasts (Fig. 3b). However, the trend was not significant ( $\chi^2$  test,  $0.2 > P > 0.1$ , d.f. = 5) owing to the presence of facilitation at relatively high target contrasts. For example, at 50% target contrast, facilitation was noted in over half of cases. Even at the highest target contrast (80%), over two-fifths of cases showed facilitation (Fig. 3b).

Psychophysical<sup>15,16</sup>, visual-evoked-potential<sup>17</sup> and modelling results<sup>11,12</sup> have indicated that weak responses are facilitated by collinear surround stimuli. We therefore investigated whether facilitation at high target contrasts occurred in cells with moderate-to-high contrast thresholds, for example, in those cells that were relatively weakly activated despite the high target contrast. Estimating the cell's contrast threshold from the target contrast–response function (Fig. 2a; and see Methods), we re-evaluated the population behaviour of the above-mentioned modulatory effects in relation to the contrast threshold of individual cells.

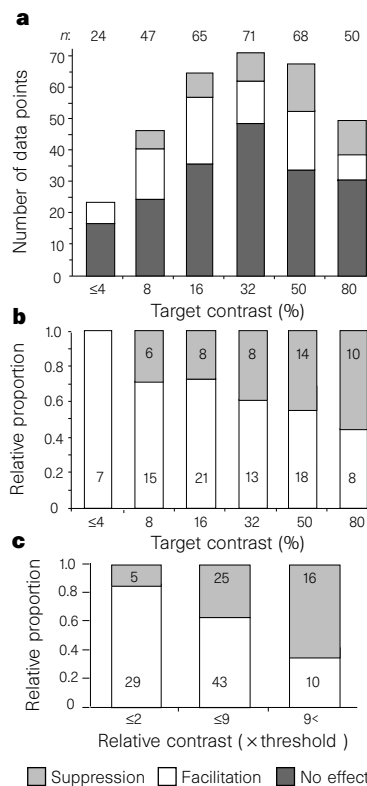
The frequency distribution of 'relative contrast' (multiples of threshold) had a large number of values around twice threshold, a

slowly declining number of measurements lying between 2 and 9 times threshold, followed by one-fifth of the sample scattered widely in a range larger than 9. Facilitative modulation was most common when the target contrast was less than or equal to twice the cell's contrast threshold. Suppression clearly dominated when the target contrast was more than nine times the threshold of individual cells (Fig. 3c). In an intermediate range of contrast (that is, more than twice, but equal to or less than nine times the threshold), the proportion of facilitative versus suppressive interactions fell in between. The effect of contrast—relative to the cell's own threshold—was highly significant ( $\chi^2$  test,  $P < 0.001$ , d.f. = 2).

Surround modulation can be orientation-related<sup>2–8,14</sup>. We thus examined the effectiveness of orthogonally oriented flanks by accumulating 150 data points from 34 cells (including 24 cells from three additional cats) in which both collinear and orthogonal flanks were tested at the same contrast values. In this population, for the collinear configuration, significant response modulation was observed in 34% of the data points (29 and 22 responses for facilitation and suppression, respectively; Table 1). With the orthogonal configuration, response modulation occurred at about the same proportion (~31%), 38 responses showing suppression and 8 responses showing facilitation. Orthogonal flanks produced an increase in the relative proportion of suppressive interactions (from ~15 to ~25%) and a decrease in facilitation (from ~19 to ~5%). Both of these effects are consistent with an overall increase in suppression with the orthogonal configuration. The pattern of crossovers from one category to another, when collinear flanks were changed to orthogonal ones, significantly favoured suppression over facilitation (Bowker's test,  $P < 0.00003$ ,  $\chi^2 = 23.85$ , d.f. = 3). Thus, suppression appears to be a substantially more general phenomenon. Facilitation, on the other hand, appears to be more specific to spatial configuration and contrast, consistent with recent psychophysical reports<sup>15,16</sup>.

A cell's contrast–response function usually comprises three regions: an accelerating nonlinear region at low contrasts, a linearly increasing region at intermediate contrasts, and a saturation region at high contrasts<sup>18</sup>. With near-threshold collinear stimuli, facilitation

**Figure 3** Population summary of contrast-dependent modulation for 325 data points, all of which satisfied the additivity test (see Methods), obtained from the 83 cells tested with three contrasts or more per cell. Data from simple and complex cells were combined using the first harmonic response for the former and the second for the latter. For unclassified cells, the dominant response was used. **a**, Frequency histogram of three types of effects; suppression (light grey), facilitation (white) and no effect (dark grey). The number of data points (each cell contributing more than once) in each of the three categories is shown for 6 values of target contrast, from the lowest, equal to or lower than 4%, to the highest, 80%. The total number of data points per contrast group is indicated at the top of each column. **b**, The proportion of facilitation and suppression is shown within the modulation group (128 data points). These data are based on 128 of 304 cases, in which contrast threshold estimates are available. The number of data points for either facilitation or suppression at each contrast range is indicated on the face of each column. The facilitative effect was common at lower target contrasts and the suppressive one at higher target contrasts. The trend was, however, not significant ( $\chi^2$  test;  $0.2 > P > 0.1$ ,  $\chi^2 = 9.21$ , d.f. = 5). **c**, Population summary of contrast threshold-dependent modulation for the same 128 data points shown in **b**. The proportion of facilitation (white bars) compared with suppression (light grey) is shown for three groups of relative contrast, expressed as multiples of the contrast threshold of the individual cells. The facilitative modulation was dominant when the target contrast was less than or equal to twice threshold, whereas suppression predominated above 9 times the threshold value. Intermediate results were obtained for relative contrasts greater than twice, but less than 9 times the threshold. The effect of relative contrast is highly significant ( $\chi^2$  test;  $P < 0.001$ ,  $\chi^2 = 14.09$ , d.f. = 2).



may prevail because of an accelerating nonlinear combination of subthreshold inputs from the flanks with weak inputs from the CRF. This integration may be based on network properties of cortical cells<sup>11,12</sup>. Facilitation near threshold may occur as the result of additional noise generated by flank stimulation<sup>11</sup> or because of excitation acting unopposed by inhibition<sup>19</sup>.

As target contrast increases, the effect of the collinear flanks reverses, becoming predominantly suppressive. Neurophysiological<sup>20,21</sup> and computational evidence<sup>11,12,22</sup> has indicated that strong, optimal stimuli elicit excitatory and inhibitory postsynaptic potential sequences, whereas only excitatory ones are detectable with weak stimuli. This means that, at high contrasts, the relative contribution of inhibitory potentials to the cell's conductance increases. Inhibitory interneurons generate spikes at twice the rate of pyramidal cells and are also less adaptable<sup>23</sup>, so the excitation–inhibition balance may be further shifted from saturation to suppression by additional subthreshold inputs from the flanks. Inputs from collinear flanks therefore appear to be combined with inputs from the CRF dynamically to regulate the cell's contrast–response function in the same way as has been proposed for thalamocortical afferents<sup>12,22</sup>.

Surround facilitation and suppression in primary visuocortical cells were first observed to be contrast-dependent with the present stimulus conditions (discrete counterphasing Gabor patches)<sup>9</sup>, consistent with results from psychophysical experiments in which comparable stimuli were used<sup>15,16</sup>. More recently, contrast-dependent surround effects were also observed when a central grating target was flanked by an annular surround<sup>10,14</sup>. The pattern of facilitation and suppression obtained with our stimulus conditions is similar to that claimed by Toth *et al.*<sup>10</sup>, but differs from that reported by Levitt and Lund<sup>14</sup>. Our stimuli mainly yielded facilitation just above the cell's contrast threshold. In their experiments<sup>14</sup>, a high-contrast annulus consistently suppressed the response to a low-contrast target inside the CRF: however, it was not clear whether their low-contrast range was near each cell's contrast threshold. The physiological results of Levitt and Lund<sup>14</sup> are similar to psychophysical results obtained by Cannon and Fullenkamp<sup>24,25</sup>, who, using the centre-annulus configuration, found that the annulus usually suppressed the perceived contrast of the central target<sup>24,25</sup>. Facilitation was noted only over a narrow range of relative contrasts between the centre and annulus<sup>25</sup>. In short, neurophysiological results emphasizing facilitation<sup>7</sup>, such as we see here, and others emphasizing suppression<sup>14</sup> complement each other, in that different configuration-specific interactions in the primary visual cortex may provide a cellular basis of psychophysical phenomena that are specific to their respective stimulus configurations.

Facilitative and suppressive centre–surround interactions may be organized differently in order to serve different functions. Facilitative interactions may be preferentially organized for collinear elements that comprise extended contours, both at moderate<sup>7</sup> and low contrasts, as in our results. Suppression is a more general phenomenon, occurring across all orientations and over a broad region around the CRF<sup>5–9,13,14</sup>. Nonspecific suppression may act to rescale the contrast–response function to maximize differential sensitivity in the face of high image contrast<sup>26</sup>. In addition, suppression that attenuates the responses of highly sensitive cells may equalize the firing rates of all cells involved in coding the same contour. The neural basis for the contextual modulation of the contrast–response function may lie in the intrinsic network of cells connected horizontally across several hypercolumns<sup>27,28</sup> or in feedback connections from higher visual areas beyond the primary visual cortex or both. Long-range lateral or feedback interactions may thus generate a second-order interaction field which constitutes an early neuronal basis of saliency, perceptual grouping and contrast scaling in vision.

*Note added in proof:* Sengpiel *et al.* (*Exp. Brain Res.* **116**, 216–228, 1997) briefly reported on collinear facilitation of a low-contrast

target by a high-contrast surround. □

## Methods

**Stimulus pattern.** The contrast of Gabor patches (mean luminance of 40 cd m<sup>-2</sup>) was periodically reversed at a rate optimal to activate the cell (1.2–6.6 Hz). Target contrast was varied between 0.5 and 80% and that of two flanks was constant at either 50 or 80%, depending on the cell's contrast threshold for the target. The target size, spatial frequency, phase and orientation were optimally fitted to the classical receptive field (CRF). The centre-to-centre separation between the target and flanks was set at 3–4 wavelengths distance (that is, the reciprocal of spatial frequency). If any responses were suspected with flanks alone, the separation was increased until the flanks alone at the distance did not produce a measurable response. The spatial phase was always the same (in-phase) between the target and flanks.

**Physiological recording.** Five adult cats were prepared for terminal physiological recording of single-cell discharges from striate cortex, using our standard procedures<sup>9,13</sup>. The cat was anaesthetized with a gas mixture of N<sub>2</sub>O : O<sub>2</sub> : CO<sub>2</sub> = 75 : 22.5 : 2.5, supplemented by continuous i.v. infusion of ~2 mg kg<sup>-1</sup> h<sup>-1</sup> pentobarbital, and paralysed with continuous i.v. infusion of 10 mg kg<sup>-1</sup> h<sup>-1</sup> gallamine triethiodide. Recordings were made within 10 deg from the projection site of the area centralis in striate cortex throughout the cortical layers. The CRF of visually responsive cells was characterized first using conventional methods<sup>9,13</sup>. Each cell was classified as simple or complex according to the original criteria of Hubel and Wiesel<sup>1</sup>.

**Data analysis and significance.** Spike counts were first obtained from peristimulus time histograms in synchrony with contrast reversal. Next, spectrum analysis was carried out using Fourier transforms. Here, we focused our analysis mainly on the first (1F) and second harmonic (2F) components as they were dominant. Error estimates and significance tests ( $P < 0.05$ ) of each harmonic component were performed by using the  $T_{\text{circ}}^2$  statistic<sup>29</sup>. For each measurement, a linear prediction of the sum of responses of target alone and the two flanks alone was compared with the measured response obtained with the three patches presented together (additivity test). When the measured response differed significantly, being either larger or smaller, from the prediction, the cell's response was considered to be modulated by the flanks. Otherwise, the cell's response was considered to be independent of the presentation of the flanks (no effect).

**Contrast threshold estimation.** The contrast threshold was extracted from the contrast–response function in two steps. An initial estimate was obtained by the sweep method<sup>30</sup>, in which contrast was incremented in 10 equally spaced logarithmic values from low to high during a stimulation period of 10 s (Fig. 2b). The slope of the first 'linear' portion of the contrast–response curve was linearly extrapolated to the noise level. Then, stimulating at 4–6 fixed contrast values (Fig. 2a) around the initial estimate, we obtained another contrast–response curve that covered a narrower range of contrasts than before. Finally, threshold was determined by executing the same linear extrapolation on the second curve. The estimated threshold always falls to the left of the point at which the response rises above noise. Insignificant values were excluded from the threshold estimate and from all subsequent analyses.

Received 3 June; accepted 20 October 1997.

- Hubel, D. H., Wiesel, T. N. Receptive fields, binocular interaction and functional architecture in the cat's visual cortex. *J. Physiol.* **160**, 106–154 (1962).
- Blakemore, C. & Tobin, E. A. Lateral inhibition between orientation detectors in the cat's visual cortex. *Exp. Brain Res.* **15**, 439–440 (1972).
- Maffei, L. & Fiorentini, A. The unresponsive regions of visual cortical receptive fields. *Vision Res.* **16**, 1131–1139 (1976).
- Nelson, J. I. & Frost, B. J. Intracortical facilitation among co-oriented, co-axially aligned simple cells in cat striate cortex. *Exp. Brain Res.* **61**, 54–61 (1985).
- Knierim, J. J. & Van Essen, D. C. Neuronal responses to static texture patterns in area V1 of the alert macaque monkey. *J. Neurophysiol.* **67**, 961–980 (1992).
- Li, C.-Y. & Li, W. Extensive integration field beyond the classical receptive field of cat striate cortical neurons—classification and tuning properties. *Vision Res.* **34**, 2337–2355 (1994).
- Kapadia, M. K., Ito, M., Gilbert, C. D. & Westheimer, G. Improvement in visual sensitivity by changes in local context: parallel studies in human observers and in V1 of alert monkeys. *Neuron* **15**, 843–856 (1995).
- Sillito, A. M., Grieve, K. L., Jones, H. E., Cudeiro, J. & Davis, J. Visual cortical mechanisms detecting focal orientation discontinuities. *Nature* **378**, 492–496 (1995).
- Mizobe, K., Polat, U., Kasamatsu, T. & Norkia, A. M. Lateral masking reveals facilitation and suppression from the same single cells in cat area 17. *Assoc. Res. Vis. Ophthalmol. Abstr.* **37**, S493 (1996).
- Toth, L. J., Rao, S. C., Kim, D.-S., Somers, D. & Sur, M. Subthreshold facilitation and suppression in primary visual cortex revealed by intrinsic signal imaging. *Proc. Natl Acad. Sci. USA* **93**, 9869–9874 (1996).

11. Stemmler, M., Usher, M. & Niebur, E. Lateral interactions in primary visual cortex: a model bridging physiology and psychophysics. *Science* **269**, 1877–1880 (1995).
12. Somers, D. C., Nelson, S. & Sur, M. Effects of long-range connections on gain control in an emergent model of visual cortical orientation selectivity. *Soc. Neurosci. Abstr.* **20**, 1577 (1994).
13. Kitano, M., Niiyama, K., Kasamatsu, T., Norcia, A. M. & Sutter, E. E. Retinotopic and nonretinotopic field potentials in cat visual cortex. *Vis. Neurosci.* **11**, 953–977 (1994).
14. Levitt, J. B. & Lund, J. S. Contrast dependence of contextual effects in primate visual cortex. *Nature* **387**, 73–76 (1997).
15. Polat, U. & Sagi, D. Lateral interactions between spatial channels: suppression and facilitation revealed by lateral masking experiments. *Vision Res.* **33**, 993–999 (1993).
16. Polat, U. & Sagi, D. The architecture of perceptual spatial interactions. *Vision Res.* **34**, 73–78 (1994).
17. Polat, U. & Norcia, A. M. Neurophysiological evidence for contrast dependent long-range facilitation and suppression in the human visual cortex. *Vision Res.* **36**, 2099–2109 (1996).
18. Albrecht, D. G. & Hamilton, D. B. Striate cortex of monkey and cat: contrast response function. *J. Neurophysiol.* **48**, 217–236 (1982).
19. Somers, D. C., Todorov, E. V., Siapas, A. G., Toth, L. J., Kim, D.-S. & Sur, M. A local circuit integration approach to understanding visual cortical receptive fields. *Cerebr. Cort.* (in the press).
20. Douglas, R. J., Martin, K. A. C. & Whitteridge, D. An intracellular analysis of the visual responses of neurones in cat visual cortex. *J. Physiol.* **440**, 659–696 (1991).
21. Hirsch, J. A. & Gilbert, C. D. Synaptic physiology of horizontal connections in the cat visual cortex. *J. Neurosci.* **11**, 1800–1809 (1991).
22. Douglas, R. J., Martin, K. A. C. & Whitteridge, D. A canonical microcircuit for neocortex. *J. Neur. Comp.* **1**, 480–488 (1989).
23. McCormick, D. A., Connors, B. W., Lighthall, J. M. & Prince, D. A. Comparative electrophysiology of pyramidal and sparsely spiny stellate neurons of neocortex. *J. Neurophysiol.* **54**, 782–806 (1985).
24. Cannon, M. W. & Fullenkamp, S. C. Spatial interactions in apparent contrast: inhibitory effects among grating patterns of different spatial frequencies, spatial patterns and orientations. *Vis. Res.* **31**, 1985–1998 (1991).
25. Cannon, M. W. & Fullenkamp, S. C. Spatial interactions in apparent contrast: individual differences in enhancement and suppression effects. *Vis. Res.* **33**, 1685–1695 (1993).
26. Heeger, D. J. Normalization of cell responses in cat striate cortex. *Vis. Neurosci.* **9**, 181–197 (1992).
27. Fitzpatrick, D. The functional organization of local circuits in visual cortex: insight from the study of tree shrew striate cortex. *Cerebr. Cort.* **6**, 329–341 (1996).
28. Gilbert, C. D. & Wiesel, T. N. Columnar specificity of intrinsic horizontal and corticocortical connections in cat visual cortex. *J. Neurosci.* **9**, 2432–2442 (1989).
29. Victor, J. D. & Mast, J. A new statistic for steady-state evoked potentials. *Electroenceph. Clin. Neurophysiol.* **78**, 378–388 (1991).
30. Norcia, A. M., Clarke, M. & Tyler, C. W. Digital filtering and robust regression techniques for estimating sensory thresholds from the evoked potential. *IEEE Eng. Med. Biol.* **4**, 26–32 (1985).

**Acknowledgements.** We thank S. P. McKee, D. Sagi, C. W. Tyler and M. Usher for helpful comments, E. Schmidt for technical support, and K. Swenson and V. Vildavski for software development. This work was supported by the National Eye Institute, the SKERF and Kyoto Prefectural University of Medicine.

Correspondence and requests for materials should be addressed to T.K. (e-mail: takuji@skivs.ski.org).

## Pathogenesis of two axonopathies does not require axonal neurofilaments

J. Eyer\*, D. W. Cleveland†, P. C. Wong‡ & A. C. Peterson§

\*INSERM C/JF 97-08 and University of Angers, CHU, 49033 Angers, France

†Ludwig Institute for Cancer Research, and Departments of Medicine and Neuroscience, University of California, San Diego, La Jolla, California 92093, USA

‡Division of Neuropathology, Department of Pathology, Johns Hopkins University School of Medicine, Baltimore, Maryland 21205, USA

§Laboratory of Developmental Biology, Molecular Oncology Group, H-5, Royal Victoria Hospital, McGill University, 687 Pine Avenue West, Montreal, Quebec, Canada H3A 1A1

Neurofilaments are a major component of the axonal cytoskeleton and their abnormal accumulation is a prominent feature of the cytopathology encountered in several neurodegenerative diseases<sup>1–8</sup>. Thus, an attractive and widely held model of pathogenesis involves the participation of disrupted neurofilaments as a common toxic intermediate<sup>9–13</sup>. Here, in direct contrast to this hypothesis, we show that two neurodegenerative disease models in the mouse, dystonia musculorum (dt)<sup>14,15</sup> and a superoxide dismutase 1 (SOD1)-mediated form of human motor neuron disease (amyotrophic lateral sclerosis, ALS)<sup>16,17</sup>, progress with little or no abatement on a transgenic background in which neurofilaments are withheld from the axonal compartment<sup>18</sup>. By specifically excluding a necessary role for axonal neurofilaments, our observations redefine the components of the pathogenic pathway leading to axon disruption in these two degenerative diseases.

We previously derived transgenic mice that accumulate a neurofilament H(NFH)- $\beta$ -galactosidase fusion protein within large projection neurons<sup>18</sup>. At low concentrations, this multivalent protein crosslinks neurofilaments in neuronal perikarya, limiting their export to axons. Despite the massive accumulation of neurofilaments in perikarya and the reduced radial growth of neurofilament-deficient axons, survival of many neuron populations is unaltered until an advanced age<sup>19,20</sup>. This surprising observation indicated that a normally distributed neurofilament cytoskeleton is not required for neuron maturation, function or extended survival and brought into question the role played by the neurofilament aggregates encountered in diverse neurodegenerative diseases. Here, to determine if axonal neurofilaments play an essential role in the pathogenesis of two murine axonopathy models, we exploited the capacity of the NFHlacZ transgene to prevent axons from being invested with a neurofilament cytoskeleton.

In the autosomal recessive disease dystonia musculorum (dt), giant axonal swellings develop in sensory neurons. The dt gene encodes BPAG1<sup>15,21</sup> and the neuronal isoform of this protein has both actin and intermediate filament-binding motifs suggesting that it may interact both with microfilaments and with neurofilaments<sup>14</sup>. Although cell bodies of sensory neurons are relatively preserved in affected mice, their axons develop swellings rich in neurofilaments (Fig. 1a, b) and degenerate, typically leading to death of affected animals by one month of age<sup>22–25</sup>. To determine if the axonal neurofilament accumulations play a role in dt pathogenesis we derived homozygous dt/dt mice bearing the NFHlacZ transgene. Eleven litters were obtained and the expected ratio of dystonic and non-affected mice (26:76) was observed. Littermates of the four expected genotypes were analysed at 7, 14, 18 and 26 days of age. In all mice bearing the NFHlacZ transgene, regardless of their genotype at the dt locus, neurofilaments were found sequestered in neuronal cell bodies whereas axons lacked a neurofilament cytoskeleton (Fig. 1c, d). Axonal swellings were counted at three levels in cervical spinal cords from affected mice, with and without the NFHlacZ transgene, on day 14, 18 and 26. The average number

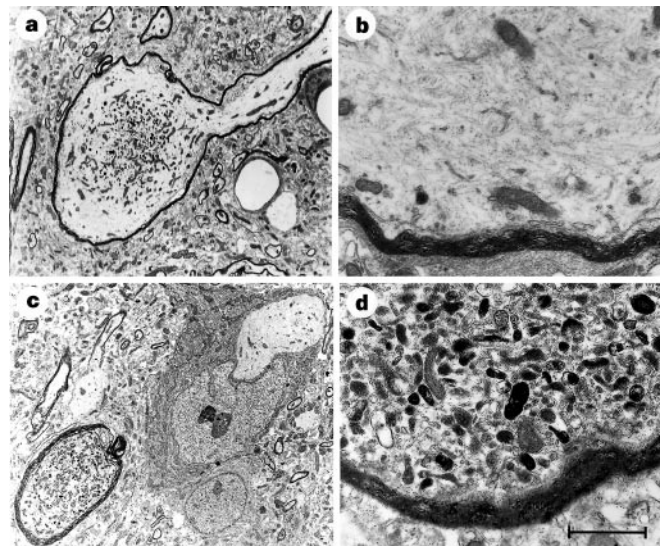


**Figure 1** Electron micrographs of typical axonal swellings in myelinated fibres in the spinal cord grey matter of dt/dt mice. **a, b**, With the NFHlacZ transgene and **c, d**, without. In non-transgenic mice, neurofilament-filled axon swellings frequently reach more than 20  $\mu$ m in diameter. Within such swellings, organelles sequester in the middle whereas filament bundles course in random directions (**b**). In contrast, expression of the NFHlacZ transgene causes neurofilaments to aggregate and remain in the cell body as seen in the cell body profile in the upper right-hand corner of **c**. In dt/dt NFHlacZ transgenic mice, axonal swellings lack neurofilaments, are smaller and are filled with vesicles and mitochondria **d**. Scale bar, 7.6  $\mu$ m (**a, c**), 1.1  $\mu$ m (**b, d**).